### Title

Delivery of thrombolytic therapy using rod-shaped plant viral nanoparticles decreases the risk of hemorrhage




### Journal

Nanoscale, 10(35)

### ISSN

2040-3364



### Authors

Pitek, Andrzej S
Park, Jooneon
Wang, Yunmei
et al.



### Publication Date

2018-09-13

### DOI

10.1039/c8nr02861c

Peer reviewed

Published in final edited form as:

*Nanoscale*. 2018 September 13; 10(35): 16547–16555. doi:10.1039/c8nr02861c.

# Delivery of thrombolytic therapy using rod-shaped plant viral nanoparticles decreases risk of hemorrhage

**Andrzej S. Pitek**[a], **Jooneon Park**[a], **Yunmei Wang**[b], **Huiyun Gao**[b], **He Hu**[a], **Daniel I. Simon**[b], and **Nicole F. Steinmetz**[a,c,d,e,f,*,#]

[a]Department of Biomedical Engineering, Case Western Reserve University, Cleveland, OH 44106, USA

[b]Harrington Heart and Vascular Institute, Case Cardiovascular Research Institute, Department of Medicine, University Hospitals Case Medical Center and Case Western Reserve University School of Medicine, Cleveland, OH 44106, USA

[c]Department of Radiology, Case Western Reserve University, Cleveland, OH 44106, USA

[d]Department of Materials Science and Engineering, Case Western Reserve University, Cleveland, OH 44106, USA

[e]Department of Macromolecular Science and Engineering, Case Western Reserve University, Cleveland, OH 44106, USA

[f]Case Comprehensive Cancer Center, Division of General Medical Sciences-Oncology, Case Western Reserve University, Cleveland, OH 44106, USA

## Abstract

Cardiovascular thrombotic disease is an underlying cause of stroke, myocardial infraction and pulmonary embolism - some of the leading causes of death worldwide. Reperfusion therapy with anticoagulant, antiplatelet, and fibrinolytic agents has significantly reduced early mortality and morbidity from acute myocardial infarction and stroke. Nevertheless, bleeding side effects (*e.g.*, intracranial hemorrhage) associated with the anti-thrombotic therapy can offset its benefits and limit its applicability to strictly defined short therapeutic windows. We have previously shown that elongated plant virus based nanoparticles can target cardiovascular thrombi and exhibited their utility for delivery of streptokinase in *ex vivo* model of thrombosis. Herein, we build upon our previous findings and demonstrate plant viral delivery of current the standard-of-care tissue plasminogen activator (tPA). Studies in a pre-clinical mouse model of arterial thrombosis indicate that while the therapeutic efficacy of free tPA and tPA-conjugated TMV is similar, the safety profile of the tPA-TMV formulation is improved, *i.e.* administration of the latter has less impact on hemostasis as demonstrated by decreased bleeding time. Thus, our data suggest that TMV-based delivery of thrombolytic therapies could be a promising and safer alternative to reperfusion therapy with tPA.

* nsteinmetz@ucsd.edu.

#present address: Department of NanoEngineering, Moores Cancer Center, University of California San Diego, La Jolla, CA 92093, USA

Conflicts of interest

There are no conflicts to declare.

## Introduction

Thrombosis can lead to fatal thromboembolism (TE), when a dislodged thrombus obstructs another site in the circulation system.[1] For example, arterial thrombi, when trapped in brain, can lead to ischemic stroke and long-lasting disability or death, while venous thrombi can travel to lung, causing pulmonary embolism and potentially fatal respiratory and cardiac failure.[2] To avoid disability and/or death, TE requires an immediate medical intervention - within few hours from the onset of disease. Standard of care relies on reperfusion therapy with anticoagulants (*e.g.*, heparin, low-molecular weight heparin, and warfarin) and/or thrombolytics (*e.g.*, tissue plasminogen activator, tPA; streptokinase, STK; and urokinase).[3, 4] Anticoagulants slow down progression of thrombi and prevent the formation of new thrombi; therefore these therapies are used for treatment for 'mild' cases of thrombosis. Only thrombolytics actively dissolve thrombi or activate patients' innate molecular pathways leading to thrombolysis; therefore only these therapeutic regimens are effective in cases of acute TE - myocardial infarction, pulmonary embolism, and ischemic stroke.[5, 6] However, both anticoagulant and thrombolytic treatments lack specificity to thrombi and affect hemostasis, which subsequently increases the risk of hemorrhage. In particular, thrombolytics such as STK or tPA, which activate circulating plasminogen (PG), can result in an systemic fibrinolysis causing life-threatening bleeding side effects.[7] To bypass these risks, thrombolytics can be delivered directly to site of disease using a drug-eluting stent or catheter.[8, 9] However, these approaches require a resource-intensive clinical setting and provide limited access to distant sites of disease (*e.g.*, ischemic stroke).

To overcome these clinical challenges, nanoparticle-based drug delivery systems have been proposed to enhance the efficacy and reduce the side effects of thrombolytic therapy.[10–22] For example, the conjugation of thrombolytic agents to liposomes or polymers (*e.g.*, polyethylene glycol or dendritic polymer) enhances efficacy due to the increase in their circulation half-lives.[13, 14, 16, 17, 20] However, prolonged circulation of thrombolytic drugs could also increase the risk of bleeding side effects. To achieve site-specific targeting, magnetically guided nanoparticle-based delivery systems have been proposed for guided delivery of thrombolytics to the site of disease, therefore reducing systemic exposure and associated side effects.[11, 12, 18, 22] Nonetheless, the translation of magnetic field-assisted nanoparticles to clinical settings remains challenging, due to the lack of effective magnetic field gradient, that are capable of imposing a high magnetic force on nanoparticles in deep blood vessels.[23] Therefore, it may be desired to design nanoparticle technologies that target sites of thrombosis based on endogenous signals and do not require external triggers.

When it comes to the design of nanoparticles for targeted drug delivery, the nanoparticle size and shape, surface chemistry (*i.e.*, charge, hydrophobicity) and surface molecular display (*i.e.*, antibodies and peptides) dictate the fate of the carrier. Among those properties, nanoparticle shape has been shown to be a critical determinant when it comes to targeting the vasculature.[24, 25] While the majority of nanoparticle-based delivery systems are of spherical shape, this may not be optimal for targeting thrombosis. Non-spherical particles (*e.g.*, disks, and rod-like elongated particles with high aspect ratios) exhibit enhanced margination, *i.e.*, lateral drift towards the walls of blood vessel.[24, 26] For example, we have

previously demonstrated that elongated, soft matter nanotubes derived from the tobacco mosaic virus (TMV) exhibit improved targeting to thrombi over spherical cowpea mosaic virus nanoparticles.[27] Furthermore, rapid clearance of TMV from circulation (circulation half-life of TMV in mice is less than 10 min)[28, 29] could potentially enhance clearance of un-utilized TMV-based drug carriers leading to improved safety profiles (*i.e.*, reduced risk of hemorrhage). Together, these data indicate potential utility of high aspect ratio TMV-based nanocarriers for development of thrombolytic therapies.

In this context, we recently reported a proof-of-concept study, in which TMV nanorods were used as a carrier to deliver STK.[19] STK-conjugated TMV retained its thrombolytic activity and exhibited enhanced efficacy compared to free STK in *ex vivo* model of thrombosis under flow conditions. However, STK is a bacterial protein and as such it is immunogenic – patients treated with STK develop neutralizing antibodies to STK. Re-administration of STK to patients with high levels of anti-STK antibody may lead to compromised efficacy and allergic reactions.[30, 31] While one might argue that also TMV is immunogenic and therefore neutralizing antibodies against TMV may hinder its use for drug delivery, we have recently shown that TMV coated with high density of non-immunogenic proteins are not neutralized by anti-carrier antibodies.[32]

Herein, we report the synthesis and characterization of TMV-based thrombolytic nanoparticles for delivery of tPA; efficacy and safety is evaluated using a combination of *in vitro, ex vivo*, and *in vivo* models of arterial thrombosis. We have selected tPA as a clot-busting agent over STK because of its clinical relevance – tPA is the only thrombolytic agent approved by FDA for reperfusion therapy. In contrary to STK, tPA has a higher specificity to fibrin (*i.e.*, one of major constituents of thrombi), allowing for increased accumulation in thrombi and localized activation of thrombolytic pathways.

## Materials and methods

### Virus propagation and purification.

TMV-Lys was propagated in *Nicotiana benthamiana* by mechanical inoculation using 5–10 μg of virus per leaf.[33] The isolation of TMV-Lys using established procedures yielded approximately 1–7 mg of virus per gram of infected leaf material.[34]

### TMV-Lys labelling with sulfo-Cyanine5.

First, alkynes were attached to TMV's carboxylic acids on the solvent-exposed surface of the channel; 100 e.q. of propargylamine (P50900; Sigma Aldrich) and 50 e.q. of EDC (25 equivalents added at 0 and 16 h; E6383; Sigma Aldrich) were added per coat protein (CP; each TMV particle consists of 2,130 identical copies of a CP unit) in 100 mM HEPES buffer, pH 7.4. The reaction was allowed to proceed for 20 h. Second, an alkyne-azide click reaction was performed by adding 1.5 e.q. of sulfo-Cyanine5 azide dye (sCy5-azide, B3330; Lumiprobe) per CP using 2 mg/mL TMV in the presence of 1 mM $CuSO_4$ (AC423615000; Fisher), 2 mM aminoguanidine (AC36891025; Fisher), and 2 mM L-ascorbic acid (AC352681000; Fisher) in 10 mM potassium phosphate (KP) buffer (pH 7.4); the reaction was allowed to proceed for 30 min on ice. TMV was purified by ultracentrifugation at

160,500 x g (42000 rpm using 50.2 Ti Rotor, Beckman Coulter) for 3 h on a 40% (w/v) sucrose cushion in 10 mM potassium phosphate (KP) buffer (pH 7.4).

### TMV-tPA synthesis.

Tissue plasminogen activator (NDC 50242–041-64; Genentech) was conjugated to the external surface of TMV-Lys using PEG spacers, using a two-step reaction:

**1)** NHS-$PEG_4$-mal linker (22104; Thermo Fisher) was added to TMV-Lys (2 mg/mL final conc.) using a 10-fold excess per CP. The reaction was carried out in 0.01 M potassium phosphate buffer pH 7.4 containing 10% (v/v) DMSO; the reaction was allowed to proceed for 3–4 h at room temperature (RT). The TMV-PEG-mal particles were then purified by ultracentrifugation at 112,000 x g (TLA-55 rotor, Beckman Coulter) for 1 hour over a 40% (w/v) sucrose cushion in 10 mM potassium phosphate buffer (KP, pH 7.4). The pellet was reconstituted to theoretical concentration of 10 mg/mL TMV-PEG in KP buffer.

**2)** tPA was conjugated via its solvent-exposed Cys side chain and Michael addition with the exposed maleimide group on TMV-$PEG_4$-mal. Lyophilized tPA was reconstituted in water to yield 1 mg/mL tPA and 35 mg/mL L-arginine, and combined with TMV-$PEG_4$-mal at 0.1 mg tPA per 1 mg TMV-$PEG_4$-mal (this equates to a molar excess of tPA per TMV of ~64). The reaction was carried overnight at RT, then particles were purified by ultracentrifugation at 112,000 x g (TLA-55 rotor, Beckman Coulter) for 1 hour over a 40% (w/v) sucrose cushion in PBS/Arg buffer, pH 7.4 (0.01 M $Na_2HPO_4$, 0.0018 M $KH_2PO_4$, 0.0027 M KCl and 0.137 M NaCl, *i.e.* PBS buffer supplemented with 35 mg/mL of arginine - A5006; Sigma Aldrich). The particles were reconstituted to a concentration of 10 mg/mL in PBS/Arg, then the un-reacted maleimide groups were quenched for 1 h at RT by addition of excess L-cysteine (168149; Sigma Aldrich). The TMV-tPA particles were then washed twice in PBS/Arg and recovered by ultracentrifugation at 112,000 x g (TLA-55 rotor, Beckman Coulter) for 1 hour over a 40% (w/v) sucrose cushion in PBS/Arg buffer, in order to remove excess L-cysteine and non-conjugated tPA. After the final washing the TMV-tPA particles were reconstituted at 10 mg/mL in PBS/Arg.

TMV-PEG control particles were prepared using the same procedure, however excluding step 2 (coupling between TMV-PEG and tPA).

### Dynamic Light scattering (DLS).

DLS measurements were performed using a 90plus instrument (Brookhaven Instruments Corporation) at a scattering angle h=90°. Reported values are averaged values of five measurements over one minute. Hydrodynamic diameters (Dh) and polydispersity indices (PDI) were calculated using the manufacturer's software.

*UV-VIS spectroscopy.* The concentrations of TMV and sCy5 dye loading were determined by the Beer-Lambert law using an extinction coefficient of TMV at 260 nm $\varepsilon_{TMV(260nm)}$ = 3.1 mL $mg^{-1}$ $cm^{-1}$ ($MW_{TMV}$ = 39.4 MDa) and extinction coefficient of sCy5 at 646 nm $\varepsilon_{Cy5(646nm)}$ = 271,000 $M^{-1}$ $cm^{-1}$ ($MW_{sCy5}$ = 747 Da).

### SDS-PAGE and Western Blot (WB).

TMV-tPA, TMV-PEG and unlabeled TMV samples (20 μg) were denatured at 100°C for 7 minutes in gel loading buffer (62.5 mM Tris-HCl pH 6.8, 2% (w/v) SDS, 10% (v/v) glycerol, 0.01% (w/v) bromophenol blue, 10% (v/v) 2-mercaptoethanol). Denatured protein samples were then separated on 4–12% NuPAGE polyacrylamide gels in 1x MOPS running buffer (Invitrogen) at 200 V for 40 min. The gels were stained with Coomassie Brilliant Blue and visualized using an AlphaImager imaging system (Biosciences).

For WB, samples separated by SDS-PAGE were transferred to nitrocellulose membranes (88018, Thermo Scientific) under a voltage of 30 V for 1 h. The membranes were then incubated at RT for 1 h in blocking solution using 5% (w/v) skimmed milk in TBST (150 mM NaCl, 10 mM Tris HCl, 0.1% (v/v) Tween-20, pH 7.5). Then, blots were incubated overnight at 4°C with: a) 0.25 μg/mL rabbit polyclonal antibody against tPA (ab47033; Abcam Biochemical) or b) 0.5 μg/mL rabbit anti-TMV antibody (custom; Pacific Immunology) in blocking solution and subsequently washed three times for 5 minutes in TBST. After washing, membranes were incubated with 0.2 μg/mL of alkaline phosphatase goat anti-rabbit antibody (G21079; Thermo Scientific) in blocking solution for 1 h at RT and washed three times for 15 minutes in TBST, and once for 5 minutes in Millipore water. Specific antibody binding was visualized using Novex AP Chromogenic Substrate (BCIP/NBT) (WP20001; Invitrogen); blots were documented using an AlphaImager imaging system (Biosciences).

### Negative staining TEM.

Particles at a concentration of 0.05 mg/mL (2 μL per grid) were adsorbed to carbon-coated copper grids (01754-F, TED PELLA), rinsed with deionized water, and negatively stained with 2% (w/v) uranyl acetate for 5 minutes before analysis with a Tecnai TF30 S/TEM at 300 kV.

### Fibrin clot thrombolysis assay.

1 mg/mL of non-PG depleted fibrinogen (Enzyme Research Labs) was polymerized with 1 IU/mL of thrombin in the presence of 3.5 mM $CaCl_2$ in PBS to form 2 mL fibrin clots in D = 35 mm petri dishes. After 3 hours, 1 μl of tPA and TMV-tPA were added in triplicates to the center and atop of the *in vitro* formed thrombus. To study efficacy, a range of concentrations of tPA were tested: 600 IU/mL, 6000 IU/mL, and 60000 IU/mL. tPA and TMV-tPA (as well as the respective controls) were allow to act on the *in vitro* formed thrombi for 15 hours; then photographs were taken to document the lysis zone.

### Carotid artery photochemical injury and thrombosis model.

All animal procedures were performed using approved protocols from the Institutional Animal Care and Use Committee at Case Western Reserve University. The CWRU tracking number is 2013–0136. TMV-conjugated tPA equivalent to a tPA dosage of 2 mg/kg of body weight (for evaluation of sCy5-TMV-tPA accumulation in thrombi) or 6 mg/kg body weight (for evaluation of therapeutic efficacy) were administered to C57BL/6 mice by tail vein injection, 5–10 minutes after injection of Rose Bengal dye at a dose of 50 mg/kg of body weight. A 1.5 mW, 540 nm green laser (Melles Griot) was used to illuminate the right

common carotid artery 5 cm from the artery to induce thrombus formation, and blood flow was monitored with a Doppler flow probe (Transonic Systems). For evaluation of sCy5-TMV-tPA accumulation in thrombi, the mice (n=3 for tPA and TMV-tPA, n=2 for TMV-PEG) were sacrificed after vessel occlusion, and the injured artery and the contralateral control were excised and fixed in formalin. sCy5 signal from *in vivo* clots (corresponding to accumulation of sCy5-TMV-tPA VNPs) was analyzed using Maestro fluorescence imaging system with yellow excitation (576 to 621 nm) and emission (635 nm long-pass) filters with automatic exposure times. For evaluation of therapeutic efficacy n=5 mice were used for PBS, tPA and TMV-tPA treatment groups and n=4 animals were used for TMV-PEG group. Doppler flow probe (MC 0.5PSL Nanoprobe, Model 0.5 VB, Transonic System) and a flow meter (Transonic Systems Model TS420) with a computerized data acquisition program (Windaq, DATAQ Instruments) were used to monitor blood flow continuously from the onset of injury until the time of blood-flow cessation (complete artery occlusion). The laser was turned off 2 minutes after complete occlusion of the vessel and the time to re-opening (if any) was monitored.

### Mouse tail bleeding assay.

Mice (n=6 for PBS and TMV control, and n=7 for free tPA and tPA-conjugated TMV) were anesthetized using pentobarbital and nanoparticle formulations were administered via retro-orbital injection with the tPA dosage of 6 mg/kg. After 5 min, the tail of a mouse (5 mm away from the tip) was transected, as described elsewhere.[35] Immediately, the transected tail was placed in PBS at 37 °C and the blood stream from the tail was carefully observed. The time to complete cessation of bleeding for 30 and 180 seconds was measured to assess the risk of thrombolytic agents.

## Results and discussion

TMV particles with solvent-exposed Lysine-158 residue (TMV-Lys)[33] were propagated and purified from *N. benthamiana* plants using previously established protocols.[34] The purification procedure yielded approximately 1–7 mg of virus per gram of used leaf material. TMV-Lys was utilized as a scaffold for bioconjugation of sulfo-Cyanine5 fluorophore (sCy5; for fluorescent imaging) and tPA (also known as alteplase and activase etc.; for thrombolytic therapy). First, azide-functionalized sCy5 (sCy5-azide) was conjugated to glutamic acids in the internal cavity of TMV-Lys utilizing a two-step reaction (Figure 1A): a) carbodiimide (*i.e.*, EDC)-based condensation reaction between the amine groups of propargylamine and TMV's glutamic acids; b) alkyne-azide cycloaddition (i.e. 'click' reaction) between sCy5-azide and alkynes installed on internal surface of TMV-Lys in step (a).[27, 29, 34] tPA was conjugated to Lys side chains exposed on the external surface of TMV-Lys using tPA's cysteine side chains. Previous studies showed that tPA contains a total of 35 cysteines, and 34 of them are assigned to 17 disulfide bonds. A single solvent-exposed cysteine-83 is therefore available for chemical modification.[36] It has also been shown that bioconjugation of tPA via Cys-83 does not significantly affect its thrombolytic activity.[37] A two-step process was utilized to conjugate tPA to TMV-Lys (Figure 1A): a) NHS ester-to-amine conjugation between polyethylene glycol (PEG)-based NHS-ester-$PEG_4$-maleimide (SM-$PEG_4$) linkers and amine groups terminating side-chain of TMV's Lysine residues; b)

maleimide-to-sulfhydryl conjugation between the thiol group terminating the Cys-83 of tPA and TMV-PEG-maleimide particles produced in step (a). The prepared particles will be referred to as sCy5-TMV-tPA or TMV-tPA.

We characterized our formulations using a variety of methods. UV-VIS measurements confirmed successful labelling of particles with sCy5 fluorophore. Based on ratio between the absorbance at 646 nm (λmax of sCy5) and 260 nm (λmax of TMV), we determined that on average 108.6 ± 11.8 sCy5 molecules were conjugated per TMV particle (Figure S1). SDS-PAGE and western blot (WB) analysis of TMV particles before and after tPA conjugation indicate covalent binding between tPA and TMV (Figure 1B). The high molecular weight (MW) bands at > 64 kDa in the TMV-tPA samples reflect the addition between the TMV capsid protein (TMVcp; MW = ~17 kDa) and tPA (apparent MW = ~57 kDa). WB analysis of sCy5-TMV-tPA conjugates confirmed presence of both TMV and tPA in >64 kDa bioconjugate bands (Figure 1C).[19, 29, 38] We estimated the amount of tPA conjugated to TMV based on densitometric analysis of gel images corresponding to 8 batches of TMV-tPA (Table S1): the ratio of high MW bands indicates that the conjugation process yielded ~90–180 μg tPA per mg TMV (or 50–100 tPA per TMV particle). However, it should be noted that this method of analysis has several flaws: i) the band density is derived from the presence of both TMVcp and tPA, given the differences in MW 17 kDa for TMVcp and 57 kDa for tPA, one may argue that the tPA content may equate to 75% of the ~ 90–180 μg tPA per mg TMV; and ii) the band intensity in the SDS gel does not scale linearly with the amount of protein loaded, which may lead to further overestimation. With the further development of protein drug-laden TMV (and other viral nanoparticles), it will be crucial to develop more accurate methods to determine protein loading per nanoparticle.

Based on theoretical calculations with tPA modelled as a 7 nm sphere, the maximum tPA coverage achieved lies at 14–15% of the TMV's surface area covered with tPA. Thus, further optimization of the chemical loading procedure may achieve up to 7x higher loading capacity.

Compared to other tPA-nanoparticle constructs, our loading efficiency falls within the large range of reported yields: various amounts of tPA loading to nanoparticles (NPs; including liposomes, PLGA polymer, silica and magnetic nanoparticles) were reported previously, ranging from 60 ng tPA per mg of NP material to 100 μg tPA per mg NP.[10, 11, 17, 18] Although the tPA loading on TMV is comparable, it does not exhaust the maximal cargo capacity of TMV because the molar ratio of tPA to TMVcp used for conjugation is ~0.03 due to high cost of the tPA. That being said, it is possible to further increase the loading of tPA on TMV. Previously, we reported conjugation of two other proteins to TMV surface: serum albumin (SA; MW = 67 kDa) and STK (MW = 47 kDa). We achieved protein loading of up to 0.35 mg SA per mg TMV and up to 0.9 mg STK per mg TMV using ≥2 excess of respective protein over TMVcp.[19, 29, 38]

TEM images of TMV-based particles (Figure 1D) revealed that TMV particles retained structural integrity after the conjugation of PEG and tPA. Dynamic light scattering (DLS) did not reveal increase in hydrodynamic diameters between TMV-Lys and TMV-PEG, and TMV-tPA (Table 1) indicating that conjugation process did not cause aggregation of TMV.

In contrary, we observed a slight decrease in hydrodynamic diameter for TMV-PEG and TMV-tPA, that could have been caused by: a) better dispersion of PEGylated TMV particles in comparison to non-modified TMV-Lys; b) fusion of several TMV-Lys particles; and/or c) possible partial fragmentation of TMV during bioconjugation and purification. In fact, all three (a, b, and c) phenomena are indicated by TEM imaging (see Figure 1D).

The thrombolytic activity of TMV-tPA was evaluated first using *in vitro* fibrin clot thrombolysis assay as described elsewhere.[19, 27] In brief, 1 mg/mL of non-PG depleted fibrinogen was polymerized by addition of 1 IU/ml of thrombin, a serine protease that cleaves fibrinogen to form insoluble fibrin that precipitates and forms a thrombus, in the presence of 3.5 mM $CaCl_2$. 0.6 to 60 IU tPA and equivalent mass of TMV-conjugated tPA formulations were spotted onto the phantom clots. The clots were imaged 15 hours after application of tPA and TMV-tPA formulations (Figure 2A) and the thrombus dissolution area was measured using ImageJ software (Figure 2B). The TMV-tPA formulations were shown to be active, although dissolved 18–34% smaller area of thrombus in comparison to free tPA (Figure 2A and B). The decreased activity of TMV-tPA may be a technical artifact due to the overestimation of tPA per TMV. However, reduced tPA activity of TMV-tPA vs. free tPA may be caused by immobilization of the enzyme on the TMV nanocarrier and/or differences in clot penetration between the small tPA and macromolecular TMV-tPA formulations. In fact, size-dependent differences in clot penetration between free and TMV-bound thrombolytic agents were previously shown to influence results of *in vitro* fibrin clot assay.[19] The reduction in thrombolytic activity of tPA after conjugation to TMV surface was significantly smaller than that of STK-conjugated TMV (*e.g.*, ~60% decrease in thrombolytic activity of STK).[19]

Next, we investigated thrombus targeting and thrombolytic efficacy using *in vivo* a photochemical injury mouse model of arterial thrombosis. Thrombosis was induced by irradiation of the right common carotid artery by 540 nm laser in wild-type C57Bl6 mice intravenously injected with Rose Bengal dye.[39] tPA control, sCy5-labeled TMV-PEG, and TMV-tPA were injected intravenously 5–10 minutes after start of irradiation by laser to simulate a clinical treatment scenario, where thrombosis is in progress before administration of therapeutics. To evaluate thrombus targeting, both injured carotid and un-injured contralateral arteries (control) were excised after complete occlusion of the vessel (indicated as ceased flow of blood in the vessel) and imaged using Maestro fluorescence imaging system (Figure 3A). The arteries from the group treated with tPA served as control for intrinsic fluorescence of the tissue and thrombi, while contralateral arteries served as control for thrombus interaction specificity (*i.e.*, to differentiate between ‘non-specific’ interaction of fluorescent particles with vascular walls and their ‘specific’ interaction with the thrombus).

Analysis of fluorescent images (Figure 3B) indicates that both TMV-PEG and TMV-tPA passively accumulate at the thrombus. We attribute the TMV-based thrombus homing to a result of TMV’s high aspect ratio and resulting flow properties. In blood stream, particles with high aspect ratios marginate towards the vessel wall, enabling increased interaction with the vascular bed, including thrombotic sites.[25, 26, 40, 41] This is in agreement with our previous observation in testing TMV-based dual modal optical-magnetic resonance imaging

agents.[27] In addition, the ratio of fluorescent signal of carotid artery to that of contralateral artery was higher in TMV-tPA group than TMV-PEG group. This indicates that the targeting specificity of TMV towards thrombi is increased after tPA conjugation, although the differences are not statistically significant. It could be speculated that the underlying cause of difference in affinity towards thrombi between TMV-tPA and TMV-PEG is the presence of fibrin-binding domains (*i.e.,* fibronectin finger-like domain and Kringle 2 domain) in the structure of tPA,[42] which enable molecular targeting of thrombi (in addition to passive targeting of TMV) by TMV-tPA particles.

To evaluate thrombolytic efficacy of TMV-tPA, we utilized the same photochemical mouse model of arterial thrombosis. After partial formation of thrombus in the artery, mice were injected with PBS (control), tPA, TMV-PEG, or TMV-tPA. First, we measured the time to complete occlusion of the vessel (indicated as ceased blood flow; Figure 4A). However, the constant formation of a thrombus in the photochemical model may not reflect the actual pathogenesis of thrombosis. Therefore, as additional measures, after complete occlusion of the artery, the laser was turned off to prevent constant formation of thrombi and i) the percentage of animals in which arteries re-opened (indicated as resumed flow of blood) as well as ii) time to re-opening of the arteries were documented in Figure 4B and C, respectively. We monitored the blood flow for a maximum of 120 minutes, after which the experiment was terminated.

During the first part of the experiment (Figure 4A) no statistically significant differences in time to complete occlusion were observed among PBS, TMV-PEG, TMV-tPA and tPA-treated mice. This can be attributed to the fact that thrombus formation in the photochemical model of arterial thrombosis is too rapid and overwhelming and appears to diminish the efficacy of tPA therapies. However, the secondary measurements provided insights into the differential activities of the samples tested: occurrence of artery re-opening events in the groups of animals treated with tPA and TMV-tPA formulations increased. Interestingly, the circulation resumed in 100% of animals treated with tPA and TMV-tPA (Figure 4B), in comparison to 60% of control animals treated with PBS and 75% of control animals treated with TMV-PEG particles (Figure 4B).

No statistically significant differences were noted comparing the tPA vs TMV-PEG vs TMV-tPA treatment arms (Figure 4C). However, it should be noted that animals without artery re-opening (in PBS and TMV-PEG groups) were excluded from ‘time to reopening’ analysis. The time to artery re-opening is not easy to interpret and could reflect either the time to thrombus dissolution (a direct effect of thrombolytic activity of formulation), or the time to ‘embolization’, when partially dislodged thrombus/embolus travels further down the artery due to high pressure of blood in the artery exerted on the wall of thrombus. Thus, apparently similar times to re-opening between TMV-PEG group and therapeutic tPA or TMV-tPA groups might not be a reflection of thrombolytic activity.

Finally, we evaluated the safety of TMV-tPA using mouse tail-bleed assays (Figure 5). PBS (control), tPA, TMV-PEG, or TMV-tPA were administered by retro-orbital injection using C57Bl6 mice (healthy mice were used for the safety studies). 5 minutes after administration of the various formulations, the mouse tails were transected and placed in a beaker

containing saline at 37°C. The time to cessation of bleeding was measured. Importantly, administration of TMV-tPA formulation did not significantly affect bleeding time in comparison to PBS control group (Figure 5), while the administration of free tPA doubled the bleeding time (*i.e.*, increased from ~423 to ~858 seconds). Thus, TMV-tPA therapy demonstrates potential to reduce the risk of bleeding associated with tPA. The reduced bleeding risk associated with administration of TMV-tPA may be attributed to the short half-life of TMV in blood circulation. It is reported that the majority of TMV particles is cleared from circulation within 10 minutes from injection and PEGylation of TMV surface does not significantly increase its circulation half-life of TMV in a mouse model.[28, 29] The short plasma presence in combination with the macromolecular presentation of tPA may reduce systemic activity of tPA, therefore decreasing the bleeding side effect.

Multiple other nanoparticle-based systems have been developed for delivery of tPA (and/or other thrombolytic molecules); these studies also showed that thrombolytic properties of tPA were not compromised by the appraoch.[10–18, 20–22] Generally, efforts focused on: 1) increasing circulation half-lives of tPA via conjugation to stealth polymers (*e.g.*, PEG) or encapsulation in liposomes;[16, 17, 20, 21] and/or 2) increasing specificity of tPA to thrombi using targeting molecules or magnetic guiding of NPs.[10–12, 27]

Using TMV nanoparticles for the development of thrombolytic agents has several advantages: (1) plant viral nanoparticles are non-pathogenic in mammals, biodegradable, and non-toxic,[44] (2) TMV nanocarriers are uniform in size and shape and contain functional groups on the surface, enabling the facile conjugation of therapeutic molecules with high degree of repeatability and precision; and (3) the high propensity of vascular margination of TMV associated with its elongated shape allows to increase efficiency of targeting to thrombus sites.[19, 25, 27] In the future, a side-by-side comparison of the various nanoparticle delivery platforms would be critical to determine the ideal design principles for delivery of thrombolytics.

## Conclusions

Due to its asymptomatic development, thrombotic diseases often remain undetected until a clinical event such as heart attack or stroke occurs. Rapid, effective, and safe therapeutic intervention is critical to avoid death and long-term disabilities. Although reperfusion therapy with fibrinolytics significantly decreases mortality, the bleeding risk followed by the administration of thrombolytics can outweigh the advantages of thrombolytic therapy. For example, in stroke, it is generally accepted that the risk of intracerebral hemorrhage offsets the benefits of thrombolytic therapy, when administered out of therapeutic window of 2–3 hours since the presentation of symptoms – in fact 2–5% of patients treated with use of thrombolytics are affected with fatal intracranial bleeding.[43] Thus, the need for safe alternatives is dire.

We utilized TMV, an elongated 300 × 18 nm soft matter nanorod, as delivery system for thrombolytic tPA. Using a mouse model of arterial thrombosis, we demonstrate

**1)** thrombus homing of the high-aspect ratio nanomaterial TMV-tPA;

2) maintained efficacy of TMV-delivered tPA; and

3) decreased bleeding of the TMV-tPA vs. tPA formulation thus indicating increased safety.

Therefore, the application of high aspect ratio plant viral-based drug delivery system may be a suitable approach for the development of next-generation thrombolytics with the reduced risk of bleeding side effects.

## Supplementary Material

Refer to Web version on PubMed Central for supplementary material.

## Acknowledgements

This work was funded in part by NIH grant R01HL137674 (to NFS). We thank Prof. Christina Wege and her team from the University of Stuttgart, Germany for the TMV-Lys mutant. Selected molecular graphics and analyses were performed with the UCSF Chimera package. Chimera is developed by the Resource for Biocomputing, Visualization, and Informatics at the University of California, San Francisco (supported by NIGMS P41-GM103311). We also appreciate Shijian Liu at Case cardiovascular research institute for the assistance of tail bleeding experiment.

## Abbreviations

| | |
|---|---|
| **TMV** | Tobacco mosaic virus |
| **TMV-Lys** | Lysine mutant Tobacco mosaic virus |
| **TMVcp** | tobacco mosaic virus capsid protein |
| **VNP** | Viral nanoparticle |
| **tPA** | tissue plasminogen activator |
| **s-Cy5** | sulfo-Cyanine 5 |
| **SDS-PAGE** | sodium dodecyl sulfate polyacrylamide gel electrophoresis |
| **WB** | western blot |
| **TEM** | transmission electron microscopy |
| **DLS** | dynamic light scattering |
| **PG** | plasminogen |
| **STK** | streptokinase |
| **TE** | thromboembolism |
| **DVT** | deep vein thrombosis |
| **PE** | pulmonary embolism |

## Notes and references


1. Benjamin EJ, Blaha MJ, Chiuve SE, Cushman M, Das SR, Deo R, Ferranti S. D. d., Floyd J, Fornage M, Gillespie C, Isasi CR, Jiménez MC, Jordan LC, Judd SE, Lackland D, Lichtman JH, Lisabeth L, Liu S, Longenecker CT, Mackey RH, Matsushita K, Mozaffarian D, Mussolino ME, Nasir K, Neumar RW, Palaniappan L, Pandey DK, Thiagarajan RR, Reeves MJ, Ritchey M, Rodriguez CJ, Roth GA, Rosamond WD, Sasson C, Towfighi A, Tsao CW, Turner MB, Virani SS, Voeks JH, Willey JZ, Wilkins JT, Wu JHY, Alger HM, Wong SS and Muntner P, Circulation, 2017, 135, e146–e603. [PubMed: 28122885]
2. Kürkciyan I, Meron G, Sterz F, Janata K, Domanovits H, Holzer M, Berzlanovich A, Bankl HC and Laggner AN, Arch Intern Med, 2000, 160, 1529–1535. [PubMed: 10826469]
3. McRae SJ and Ginsberg JS, Circulation, 2004, 110, I-3–I-9. [PubMed: 15339875]
4. Wells PS, Forgie MA and Rodger MA, JAMA, 2014, 311, 717–728. [PubMed: 24549552]
5. Chatterjee S, Chakraborty A, Weinberg I, Kadakia M, Wilensky RL, Sardar P, Kumbhani DJ, Mukherjee D, Jaff MR and Giri J, JAMA, 2014, 311, 2414–2421. [PubMed: 24938564]
6. Rutherford JD and Braunwald E, Chest, 1990, 97, 136S–145S. [PubMed: 2108851]
7. Ali MR, Salim Hossain M, Islam MA, Saiful Islam Arman M, Sarwar Raju G, Dasgupta P and Noshin TF, The Scientific World Journal, 2014.
8. Matsuda T, Journal of Controlled Release, 2002, 78, 125–131. [PubMed: 11772454]
9. Ong ATL and Serruys PW, Nature Reviews Cardiology, 2005, 2, 647.
10. Chen J-P, Yang P-C, Ma Y-H, Tu S-J and Lu Y-J, Int J Nanomedicine, 2012, 7, 5137–5149. [PubMed: 23055726]
11. Chen J-P, Yang P-C, Ma Y-H and Wu T, Carbohydrate Polymers, 2011, 84, 364–372.
12. Chung T-W, Wang S-S and Tsai W-J, Biomaterials, 2008, 29, 228–237. [PubMed: 17953984]
13. Heeremans JL, Prevost R, Bekkers ME, Los P, Emeis JJ, Kluft C and Crommelin DJ, Thromb. Haemost, 1995, 73, 488–494. [PubMed: 7667833]
14. Heeremans JLM, Gerrttsen HR, Meusen SP, Mijnheer FW, Panday RSG, Prevost R, Kluft C and Crommelin DJA, Journal of Drug Targeting, 1995, 3, 301–310. [PubMed: 8821004]
15. Kempe H and Kempe M, Biomaterials, 2010, 31, 9499–9510. [PubMed: 20732712]
16. Kim I-S, Choi H-G, Choi H-S, Kim B-K and Kim C-K, Arch. Pharm. Res, 1998, 21, 248–252. [PubMed: 9875439]
17. Kim J-Y, Kim J-K, Park J-S, Byun Y and Kim C-K, Biomaterials, 2009, 30, 5751–5756. [PubMed: 19656559]
18. Ma Y-H, Wu S-Y, Wu T, Chang Y-J, Hua M-Y and Chen J-P, Biomaterials, 2009, 30, 3343–3351. [PubMed: 19299010]
19. Pitek AS, Wang Y, Gulati S, Gao H, Stewart PL, Simon DI and Steinmetz NF, Mol. Pharmaceutics, 2017, 14, 3815–3823.
20. Rajagopalan S, Gonias SL and Pizzo SV, J Clin Invest, 1985, 75, 413–419. [PubMed: 3156148]
21. Sakuragawa N, Shimizu K, Kondo K, Kondo S and Niwa M, Thrombosis Research, 1986, 41, 627–635. [PubMed: 3961739]
22. Tadayon A, Jamshidi R and Esmaeili A, International Journal of Pharmaceutics, 2015, 495, 428–438. [PubMed: 26363110]
23. Singh D, McMillan JM, Kabanov AV, Sokolsky-Papkov M and Gendelman HE, Nanomedicine (Lond), 2014, 9, 501–516.
24. Doshi N, Prabhakarpandian B, Rea-Ramsey A, Pant K, Sundaram S and Mitragotri S, Journal of Controlled Release, 2010, 146, 196–200. [PubMed: 20385181]
25. Toy R, Hayden E, Shoup C, Baskaran H and Karathanasis E, Nanotechnology, 2011, 22, 115101. [PubMed: 21387846]
26. Lee S-Y, Ferrari M and Decuzzi P, Nanotechnology, 2009, 20, 495101. [PubMed: 19904027]
27. Wen AM, Wang Y, Jiang K, Hsu GC, Gao H, Lee KL, Yang AC, Yu X, Simon DI and Steinmetz NF, J. Mater. Chem. B, 2015, 3, 6037–6045. [PubMed: 26509036]

28. Bruckman MA, Randolph LN, VanMeter A, Hern S, Shoffstall AJ, Taurog RE and Steinmetz NF, Virology, 2014, 449, 163–173. [PubMed: 24418549]
29. Pitek AS, Jameson SA, Veliz FA, Shukla S and Steinmetz NF, Biomaterials, 2016, 89, 89–97. [PubMed: 26950168]
30. Elliott JM, Cross DB, Cederholm-Williams SA and White HD, The American journal of cardiology, 1993, 71, 640–645. [PubMed: 8447258]
31. Lee HS, Yule S, McKenzie A, Cross S, Reid T, Davidson R and Jennings K, European heart journal, 1993, 14, 1640–1643. [PubMed: 8131761]
32. Gulati NM, Pitek AS, Czapar AE, Stewart PL and Steinmetz NF, J. Mater. Chem. B, 2018, DOI: 10.1039/C7TB03106H.
33. Geiger FC, Eber FJ, Eiben S, Mueller A, Jeske H, Spatz JP and Wege C, Nanoscale, 2013, 5, 3808–3816. [PubMed: 23519401]
34. Bruckman MA and Steinmetz NF, Virus hybrids as nanomaterials: methods and protocols, 2014, 173–185.
35. Wang Y, Fang C, Gao H, Bilodeau ML, Zhang Z, Croce K, Liu S, Morooka T, Sakuma M and Nakajima K, J Clin Invest, 2014, 124, 2160. [PubMed: 24691441]
36. Wu S-L, Jiang H, Hancock WS and Karger BL, Anal. Chem, 2010, 82, 5296–5303. [PubMed: 20481521]
37. McCarthy JR, Sazonova IY, Erdem SS, Hara T, Thompson BD, Patel P, Botnaru I, Lin CP, Reed GL and Weissleder R, Nanomedicine, 2012, 7, 1017–1028. [PubMed: 22348271]
38. Gulati NM, Pitek AS, Steinmetz NF and Stewart PL, Nanoscale, 2017, 9, 3408–3415. [PubMed: 28112764]
39. Furie B and Furie BC, Journal of Clinical Investigation, 2005, 115, 3355. [PubMed: 16322780]
40. Geng Y, Dalhaimer P, Cai S, Tsai R, Tewari M, Minko T and Discher DE, Nature nanotechnology, 2007, 2, 249–255.
41. Gentile F, Chiappini C, Fine D, Bhavane RC, Peluccio MS, Cheng MM-C, Liu X, Ferrari M and Decuzzi P, Journal of Biomechanics, 2008, 41, 2312–2318. [PubMed: 18571181]
42. Van Zonneveld A, Veerman H and Pannekoek H, Journal of Biological Chemistry, 1986, 261, 14214–14218. [PubMed: 3021732]
43. Miller DJ, Simpson JR and Silver B, The Neurohospitalist, 2011, 1, 138–147. [PubMed: 23983849]
44. Soenen SJ, Rivera-Gil P, Montenegro J-M, Parak WJ, De Smedt SC and Braeckmans K, Nano today, 2011, 6, 446–465.
45. Namba K, Pattanayek R and Stubbs G, Journal of molecular biology, 1989, 208, 307–325. [PubMed: 2769760]
46. Pettersen EF, Goddard TD, Huang CC, Couch GS, Greenblatt DM, Meng EC and Ferrin TE, Journal of computational chemistry, 2004, 25, 1605–1612. [PubMed: 15264254]

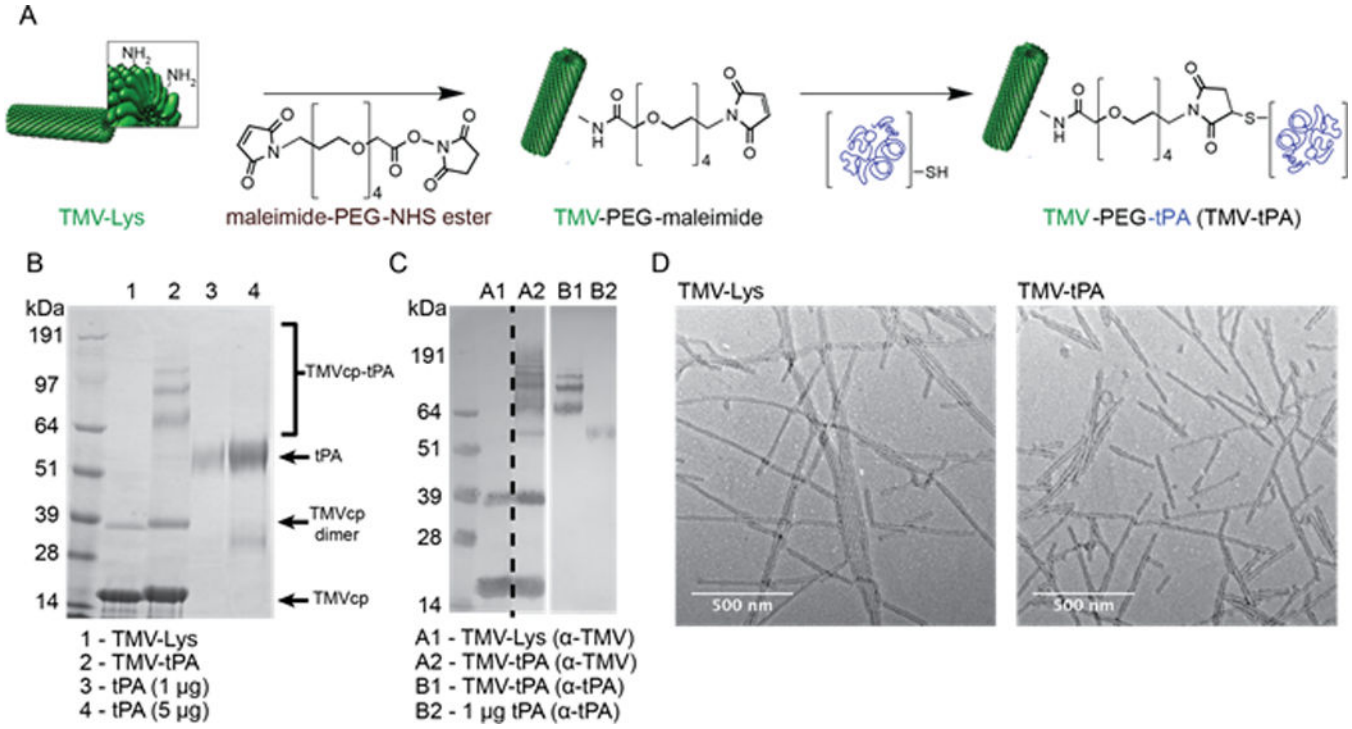


**Figure 1. TMV-tPA bioconjugation and characterization.**

A, Schematic of bioconjugation between TMV-Lys and tPA. TMV's structural data (ID: 2TMV)[45] obtained from the Protein Data Bank (PDB) was used to represent these components using UCSF Chimera software.[46] B, SDS-PAGE analysis of TMV-Lys particles before and after conjugation of tPA. Bands corresponding to TMVcp (MW = ~17 kDa), TMVcp dimer (MW = ~34 kDa) and tPA (apparent MW = ~57 kDa) are indicated with arrows. The TMV-tPA bioconjugates are visible as the high molecular weight protein bands (apparent MW > 64 kDa). C, Western Blot analysis confirms that protein bands larger than 64 kDa consist of TMVcp and tPA. D, TEM images of TMV-Lys and TMV-tPA.

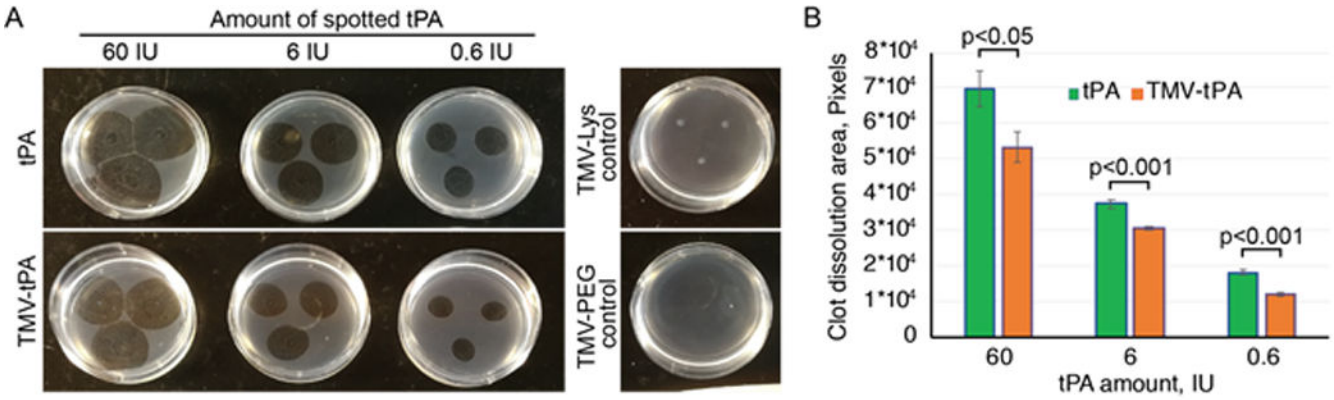


**Figure 2. TMV-tPA *in vitro* assay of thrombolytic activity: phantom clot dissolution.**

A, Image of phantom clots 15 hours after application of tPA and TMV-tPA (samples were applied in triplicates). The dark circular zones result from thrombolysis of fibrin matrix by tPA. B, Quantification of area-of-dissolution in image A. 2-tailed, unpaired student's T-test was used to calculate the p-values; $p<0.05$ indicates statistically significant differences.

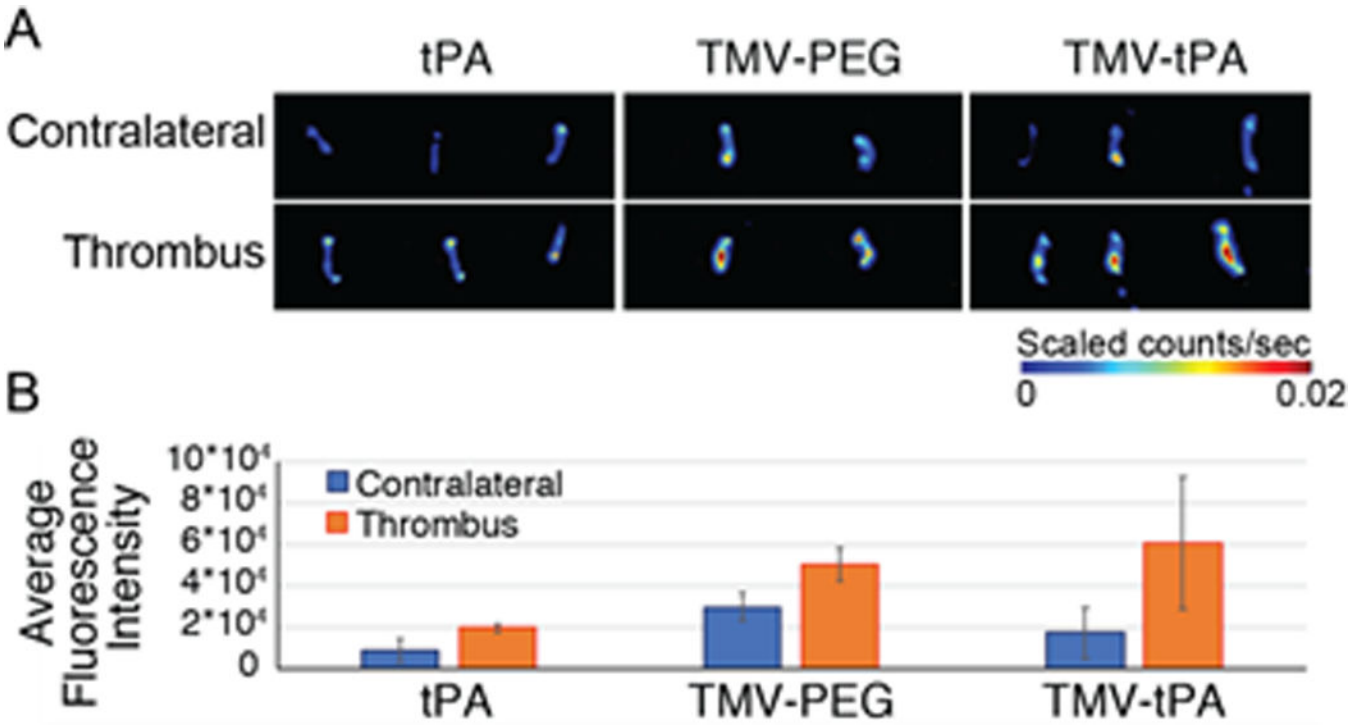


**Figure 3.** ***In vivo*** **evaluation of passive targeting of thrombi by TMV-tPA particles in photochemical model of arterial thrombosis.**

A, Fluorescent images of carotid arteries (containing thrombi) and contralateral arteries (no thrombus) excised from mice exposed to tPA (control), and fluorescent TMV-PEG and TMV-tPA particles. B, Quantification of TMV accumulation in thrombi – quantification of sCy5-TMV-PEG/tPA fluorescent signal in image of panel A. The observed differences between fluorescence of thrombus vs contralateral artery were not statistically significant for TMV-PEG and TMV-tPA. Given natural variability of immune response between individual animals to TMV that could result in variable clearance rates, we expect differences in the content of TMV-based formulations in thrombi between animals leading to high standard deviation. The difference between fluorescence of thrombus vs contralateral artery observed in tPA group was likely due to autofluorescence of thrombi (not present in contralateral artery) and leak of fluorescence of rose bengal dye trapped in thrombus through emission filter used during imaging (635nm long pass).

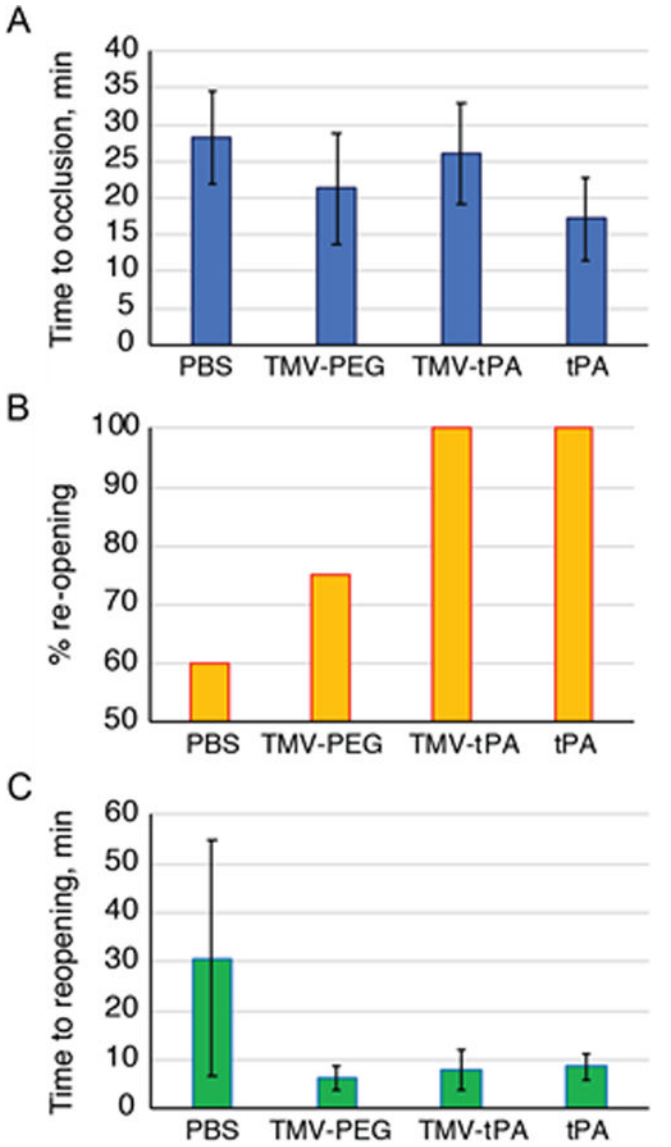


**Figure 4. Evaluation of TMV-tPA thrombolytic activity *in vivo* in photochemical model of arterial thrombosis.**

A, Time to complete occlusion of carotid artery (cessation of blood flow) in mice after induction of arterial thrombosis via photochemical injury and intravenous treatment with PBS (control), TMV-PEG, TMV-tPA and tPA. B, Fraction of mice with circulation in carotid artery resumed (artery re-opening) within 120 minutes after complete occlusion and cessation of irradiation with laser. C, Time to re-opening of carotid artery after complete occlusion and cessation of irradiation with laser (animals without artery re-opening within 120 minutes were excluded from this analysis).

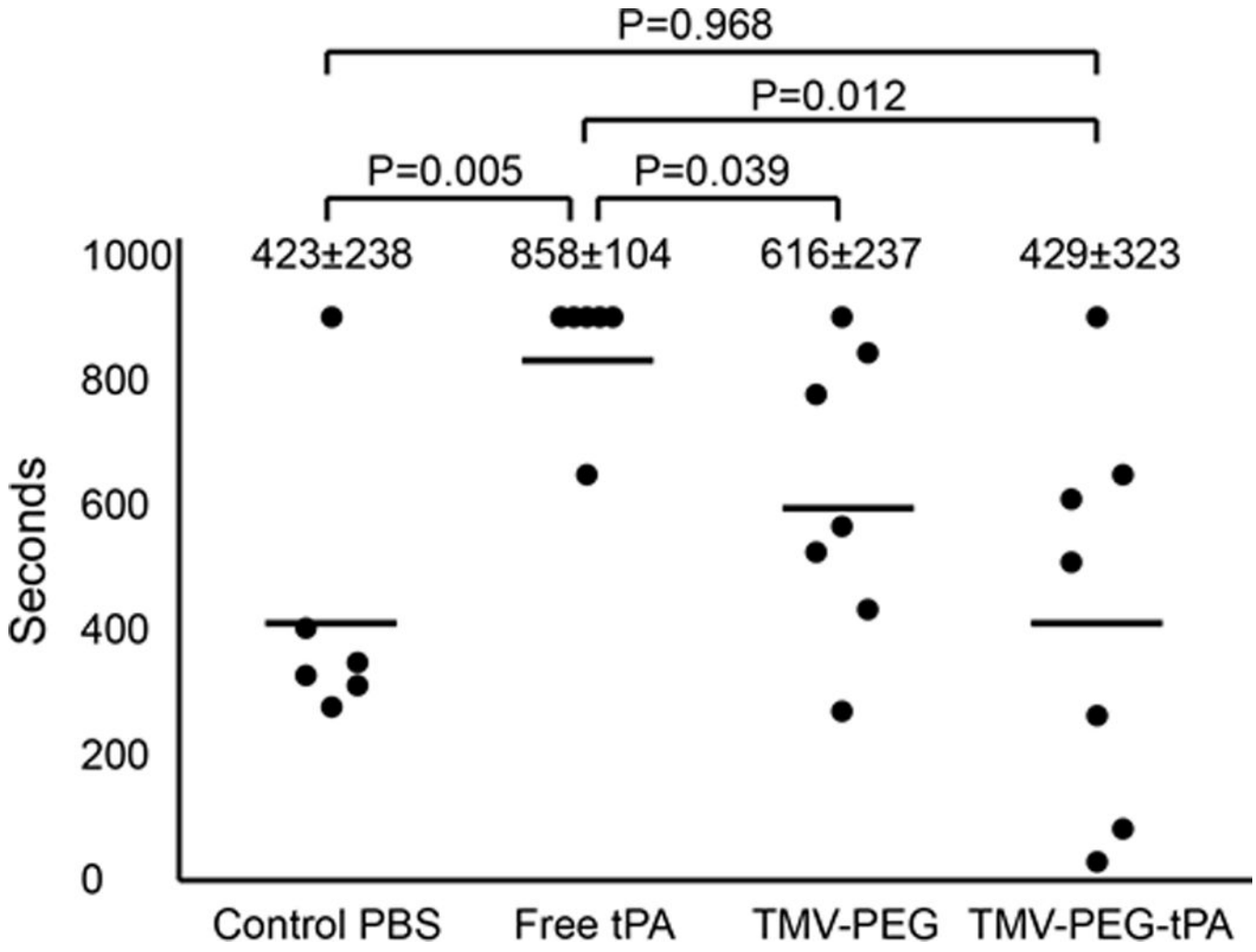


**Figure 5. *In vivo* evaluation of bleeding side effects of TMV-based thrombolytic formulations by mouse tail bleeding.**

There was no statistically significant difference of tail-bleeding time between control PBS and TMV-tPA treated groups. However, the administration of free tPA significantly increased the average time to cessation, which indicates the low specificity and high risk of haemorrhage associated with tPA.

**Table 1.**

DLS measurements of TMV bioconjugates.

| Sample | Dh, nm | SD, nm | PDI |
|---|---|---|---|
| **TMV-Lys** | 251.0 | 3.2 | 0.23 |
| **TMV-PEG** | 206.8 | 1.9 | 0.19 |
| **TMV-tPA** | 172.1 | 2.4 | 0.24 |